Biophysical Chemistry 177–178 (2013) 24–33

Contents lists available at SciVerse ScienceDirect

Biophysical Chemistry

journal homepage: http://www.elsevier.com/locate/biophyschem

Characterization of the nucleation process of lysozyme at physiological pH: Primary but not sole process

Giovanna Navarra [a,*], Filippo Troia [a], Valeria Militello [a,b], Maurizio Leone [a,b]

[a] Dipartimento di Fisica e Chimica, Università di Palermo, Via Archirafi 36, 90123 Palermo, Italy
[b] Istituto di Biofisica, CNR, Via Ugo La Malfa 153, 90146 Palermo, Italy

HIGHLIGHTS

- We study the molecular mechanisms involved in lysozyme aggregation at pH 7.4.
- Nucleated and non-nucleated processes contribute to aggregate growth.
- Their extent is regulated by the protein concentration.
- Globular aggregates grow without formation of intermolecular β-sheets.
- During fast cooling, heated lysozyme is not stable: aggregation may proceed.

GRAPHICAL ABSTRACT

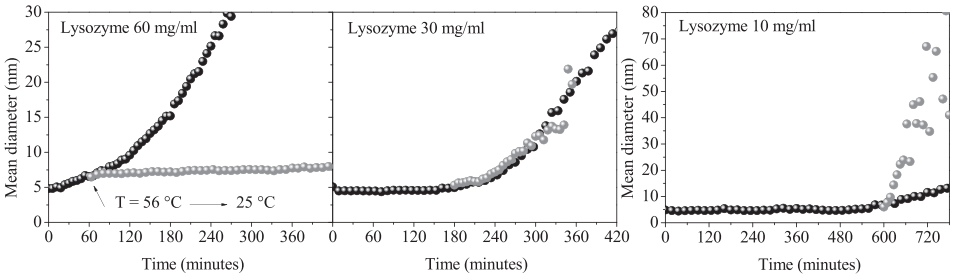

ARTICLE INFO

Article history:
Received 20 December 2012
Received in revised form 14 March 2013
Accepted 19 March 2013
Available online 3 April 2013

Keywords:
Protein aggregation
Nucleation process
Dynamic light scattering
FTIR spectroscopy
AFM

ABSTRACT

We report on a kinetic study of the heat-induced aggregation process of lysozyme at physiological pH. The time evolution of the aggregation extent and the conformational changes of the protein were followed by dynamic light scattering (DLS) and FTIR spectroscopy, respectively, whereas the morphology of the aggregates was observed by Atomic Force Microscopy (AFM). The conformational changes of the secondary and tertiary structures were simultaneous and distinct in time with respect to the formation of aggregates. Oligomer formation occurred through at least two different aggregation processes: a nucleation process and a homogeneous non-nucleative diffusion-controlled process. FTIR measurements showed that supramolecular aggregation proceeded without the formation of β-aggregated structures and AFM images revealed the presence of oligomers and amorphous aggregates; no fibrillar structures were observed.

1. Introduction

Protein aggregation processes are an important issue in several scientific fields, from medicine to clinical and industrial technologies. Knowledge of the molecular basis for these processes allows proper control and design of the protein aggregates to be achieved [1]. On the one hand, this is important in making biomaterials, with potential applications for food texture [2], in tissue engineering or as cellular scaffolds [3–5]. On the other hand, protein aggregation state and structural properties, especially when the proteins are implicated in neurodegenerative diseases and cellular toxicity processes, are important areas for current study [6–11]. Various kinds of aggregate states have been identified and defined: oligomers with low or high molecular weight, nucleus, seed, protofibril, protofilament, fibril and amyloid [11–17]. The aggregation processes are usually accompanied by conformational changes of the native protein, leading to different aggregate structures [11,16–20]. Other findings indicate that specific soluble oligomers of protein, precursors of insoluble amyloid fibrils, are the toxic species [10,11,21–23]. In particular, these oligomers have a high degree of hydrophobicity and

* Corresponding author. Tel.: +39 091 23891772.
E-mail address: giovanna.navarra@unipa.it (G. Navarra).

0301-4622/$ – see front matter © 2013 Elsevier B.V. All rights reserved.
http://dx.doi.org/10.1016/j.bpc.2013.03.004

high β-sheet structure content [6,8,24,25]. Under appropriate conditions, oligomers with these structural characteristics can evolve to form protofibrils and amyloid fibrils, as proven by x-ray diffraction patterns and by birefringence [26].

Several models for amyloid formation have been suggested [17,27–31]. One of these consists in the "primary nucleation model", in which the conversion of protein monomers into fibrillar structures occurs via transiently populated aggregation nuclei acting as bottlenecks, that limit the rate of fibril formation. Afterwards, elongation and thickening proceed by addition of monomers, or oligomers and further associations of already formed fibrils.

Lysozyme is constituted by 129 residues and made up of two domains (α and β) cross-linked with four disulfide bridges [32]. Some peculiar characteristics (well-known 3D structure, thermodynamic stability, folding mechanism, and ability to form amyloid fibrils) make this protein an excellent model for characterizing intermediate species and for studying the mechanisms underlying aggregation processes, such as nucleation and protein–protein interaction [25,31–38].

Lysozyme is known to self-assemble to form various supramolecular structures, depending on the thermodynamic and environmental conditions. At moderately acid pH and ionic strength, lysozyme solutions may undergo a liquid–liquid phase separation [39,40], facilitating the formation of crystals [41,42]. Also, through a nucleation process, at low pH, lysozyme is able to assemble into amyloid fibrils upon heating [33–36], or upon addition of alcohol or other denaturant agents [43–46]. Besides, at 80 °C and pH 7, it forms non-fibrillar aggregates that, at a submicron length scale, appear as compact ellipsoidal objects with a length from about ten nanometers to a few microns [47]. Near the isoelectric point, lysozyme aggregates by cluster–cluster associations with a diffusion-limited regime [48].

In this study, light scattering experiments involving a sample cooling (known here as thermal quenching experiments) revealed a nucleation process leading to the formation of non-fibrillar aggregates of lysozyme at physiological pH. In particular, we studied the heat-induced aggregation process of hen egg white lysozyme at pH 7.4 in samples with different concentrations, exploring the mechanisms underlying aggregation. Different techniques were used, such as Fourier Transform Infrared absorption (FTIR) and dynamic light scattering (DLS). FTIR was used to identify the protein conformational changes, whereas DLS provided information on particle dimension distribution and growth [31,49]. Moreover, we report thermal quenching experiments carried out using DLS to monitor the evolution of heat-induced protein aggregation after sample cooling. The morphology of the oligomeric aggregates formed in the first steps of lysozyme aggregation was characterized by atomic force microscopy (AFM). This study highlighted the occurrence of a nucleation process simultaneous to a non-nucleative mechanism not leading to formation of lysozyme fibrillar aggregates but to amorphous aggregates composed of high molecular weight oligomers.

2. Materials and methods

2.1. Materials

Hen egg white lysozyme was obtained from SIGMA (crystallized and lyophilized, L-6876, Lot 114 K0626, purity ≥90%). All solutions were freshly prepared with phosphate buffer (PB) 0.1 M at pH 7.4. The protein solutions were sterile-filtered with 0.1 μm filter (Sartorius, no 16553). Deuterated samples were prepared for infrared absorption measurements. Protein solutions were prepared at different concentrations: 10 (SolA), 20 (SolB), 30 (SolC) and 60 (SolD) mg/ml. The concentration in different samples was determined by absorption measurements performed with a UV-2401PC Shimadzu spectrophotometer; the molar extinction coefficient used for the concentration estimate in the Lysozyme was $\varepsilon_{280} = 36{,}000\ M^{-1}\ cm^{-1}$ [35].

2.2. Dynamic light scattering

Quantitative information on the growth of macromolecular assemblies in solution was obtained by dynamic light scattering (DLS) during the aggregation pathway, using a NanoS Zetasizer (Malvern Instruments). It was equipped with a He–Ne laser (λ = 633 nm, 4 mW), using a scattering angle of 173°. The sample compartment was self-enclosed and the internal temperature was automatically controlled. The most important information on the aggregation state of proteins obtained with DLS was given by the scattered light intensity, by the Z-average (a measure of the mean diameter) and by the diameter distribution of the particles in solution. Two approaches were utilized to obtain size information from the correlation function (see details in Navarra et al. [16]): a) fitting a single exponential to the correlation function to obtain the mean size (Z-average diameter), that is the weighted mean hydrodynamic size of the ensemble collection of particles measured by DLS (an increase in Z-average value is an index of particle aggregation); b) fitting a multiple exponential to the correlation function to obtain the distribution of particle sizes (CONTIN analysis). The latter analysis procedure was used to obtain the distribution of the particle dimensions in the protein solution, based on the total light scattering intensity at different specific times of the whole kinetics. Protein aggregation occurring on each sample was monitored kinetically at 56 °C. Then, a suitable experimental method of thermal quenching was carried out by DLS. This consisted in acquiring kinetics at 25 °C after sample incubation at 56 °C for different times. We stopped the thermal aggregation at specific time points during the kinetics, bringing samples to 25 °C and then monitoring the kinetics at this lower temperature. The time point was chosen for each sample as the moment when the Z-average increased markedly (when the slope of the tangent to the curve became positive). This was done so as to study the evolution of aggregation at room temperature after incubation at 56 °C (hereinafter we refer to this experimental method as thermal quenching experiments).

2.3. FTIR spectroscopy

The conformational changes of the lysozyme samples were followed by acquiring FTIR spectra at different times, using a Bruker Vertex 70 spectrometer. This instrument operates in the mid-IR spectral range with a globar light source (i.e. a U-shaped silicon carbide element) and with a spectral resolution of 2 cm^{-1}. Each spectrum was averaged over 100 scans. The errors associated with determining the position and amplitude of the IR bands were $\pm 1\ cm^{-1}$ and less than 1%, respectively. The absorption spectrum of the sample-holder (CaF_2 windows) was subtracted from the spectrum of each sample, while the contribution from buffer absorption was eliminated by the analysis procedure leading to difference spectra. The resultant spectra were smoothed with a 13-point Savitzky–Golay function. D_2O solutions were used to avoid the spectral overlaps between the Amide I band and the strong absorption band of the water at about 1640 cm^{-1}, and to monitor the H–D exchanges by the Amide II and the Amide II′ bands [50]. Deuterated samples were placed between two CaF_2 windows, with a 0.05 mm Teflon spacer.

The infrared zones investigated were the regions of the Amide I and Amide II bands. The Amide I band, that in D_2O is called Amide I′ for the shifts towards 1650 cm^{-1}, is due to an out-of-phase combination of the C═O and C–N stretching modes of the amide groups. Generally, it has a composite profile consisting of several spectral components related to the different types of secondary structures [51–54]. The main band at $1655 \pm 1\ cm^{-1}$ in the Amide I region was assigned to α-helices, bands at 1672 ± 1 and $1681 \pm 1\ cm^{-1}$ reflected the contribution from β-turns, and the band at $1636 \pm 1\ cm^{-1}$ was assigned to β-sheets. In general, further information on the intermolecular aggregation (β-aggregates) can be obtained from two components at about 1620 and 1680 cm^{-1} [55] due to vibrations of the carboxylic groups in β-sheets of intermolecular structures [18]. As regards the Amide II

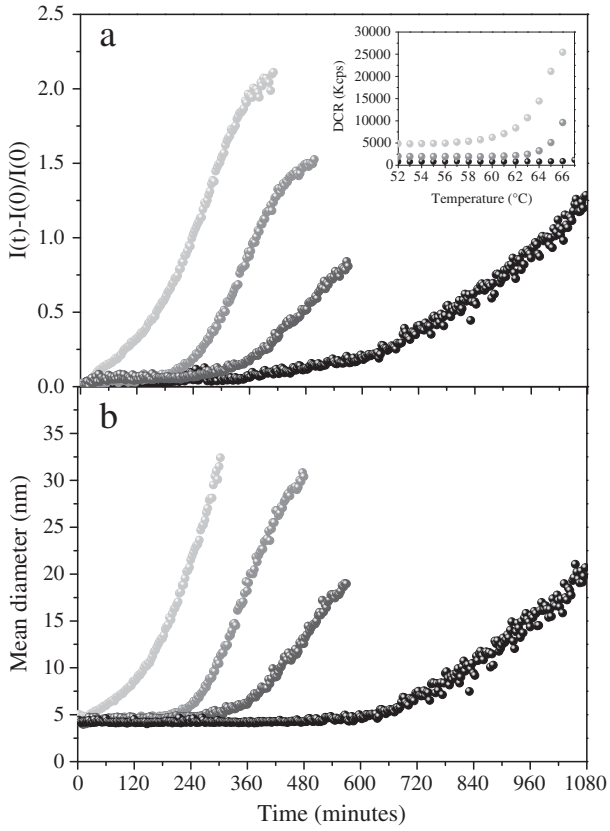

Fig. 1. Time evolution of a) the normalized scattering light intensity and b) mean diameter of the particles in solution at different protein concentrations: 10 mg/ml — SolA (●); 20 mg/ml — SolB (◉); 30 mg/ml — SolC (◍); 60 mg/ml — SolD (○) samples. The pH value was 7.4 and the temperature was 56 °C. The inset shows the scattered light intensity (derived count rate, DCR) measured by scanning the temperature (see text). The different value of the initial DCR was due to the different sample concentration. The experimental error is smaller than the symbol size.

(or II′) band (1400–1580 cm^{-1}), it is predominantly associated with the N–H (or D) in-plane bending of the peptide groups [56]. When H–D exchange occurs, a simultaneous increase in Amide II′ and decrease in Amide II is observed. In order to identify the time evolution of each spectral component under the broad amide bands, difference spectra were obtained by subtracting from the spectrum at a generic time t, the spectrum at t_0 (where t_0 was 7 min after the beginning of the experiment to reach thermal equilibrium):

$$\Delta Abs(t,\upsilon) = Abs(t,\upsilon) - Abs(t_0,\upsilon).$$

This method highlighted the changes on the various components during the evolution of the infrared absorption kinetics and simultaneously removed from the spectrum the contribution due to the buffer absorption unchanged with the time.

2.4. Atomic force microscopy

In order to characterize the morphology of the supramolecular assemblies during the aggregation pathway, atomic force microscopy (AFM) measurements were carried out on native and aggregated Lysozyme. At specific incubation times, lysozyme aliquots were drawn and immediately cooled to −20 °C in order to prevent the morphology of the samples from modifying due to any evolution in the aggregation process that might occur at room temperature. For the AFM images, lysozyme solutions at room temperature were appropriately diluted in bi-distilled demineralized water according to their concentration: the 10 mg/ml sample was diluted 1:400, whereas the 60 mg/ml sample was diluted 1:800. A small aliquot (10 μl) of protein solution was deposited on freshly cleaved mica. The samples were dried overnight by a gentle nitrogen flux and imaged in air. An AFM height signal was recorded. It was accompanied by the acquisition of the phase and amplitude error signals. The instrument used for the AFM measurements in tapping mode was a Veeco MultiMode V Scanning Probe Microscope. Etched-silicon probes with Al-coating on the detector side having a pyramidal-shape tip with a nominal curvature <10 nm were used. During scanning, the 125 ± 10 μm long cantilever, with a nominal spring constant in the range of 40 N/m, oscillated at its resonance frequency (330 kHz). Height, phase and amplitude error images were collected by capturing 512 × 512 points in each scan, and the scan rate was maintained below 1 line per second. The deterioration of the tips was monitored by using a test pattern before and after each measurement session.

3. Results

3.1. Aggregation process

3.1.1. Aggregate growth

In Fig. 1, the scattered light intensity and the mean diameter of the protein molecules in solution, when incubated at 56 °C, are shown as a function of time. The choice of this temperature deserves some comment. It is well known that protein concentration markedly affects the temperature at which aggregate growth is activated. Thus, in order to determine the appropriate temperature for the kinetic studies, temperature scans on samples having different concentrations were made (see the inset of Fig. 1). The aggregation process of the most concentrated sample (SolD) was activated before 56 °C, while the crucial temperature was just lower than 66 °C for SolA sample. Therefore, the temperature chosen for incubation was 56 °C for all the samples.

The data in Fig. 1 show the presence of a clear lag phase in the time evolution of the kinetics in the case of the SolA, SolB and SolC samples, whose extension decreased when the concentration increased. In the case of the SolD sample, it was not possible to affirm or to exclude the presence of a lag phase: the growth was rapid and, as a consequence, the lag phase could be hidden by the quick onset of growth due to the high concentration of molecules. Lag phase is a feature of nucleation processes and is generally indicated as the time necessary for the proteins to undergo the conformational changes and to interact with each other to form the so-called fibrillation nucleus [27,57,58].

In general, the time necessary to undergo the conformational changes before the formation of nuclei is independent of protein concentration because they occur on single molecules, whereas the formation of nuclei is a process dependent on protein concentration [58]. From Fig. 1a, the dependence of the lag phase on the protein concentration was clear; this necessarily indicated that fulfillment of the conformational changes before aggregate formation was not the only reason for the presence of the lag phase. Indeed, the increase in the intensity of the light scattered by the SolA sample between 360 and 600 min (Fig. 1a), accompanied by a very low increase in the mean dimension of the molecules in solution (Fig. 1b), indicated that some oligomers were forming in solution. After 600 min, a remarkable increase in the mean diameter of SolA molecules was observed, indicating that the growth of supramolecular aggregates had started. On analyzing the trend of the intensity of scattered light and of the mean diameter in other samples, the same mechanism was observed for SolB and SolC. Finally, the time evolution of the mean diameter in SolD showed the absence of a clear lag phase and a sudden growth in mean diameter after a few minutes of incubation, due to the high protein concentration. As expected, our data show that the rate of the growth step occurring at 56 °C increased with an increase in initial monomer concentration in solution.

In order to obtain more information on the different mechanisms that contribute to the lag phase, the evolution of aggregate growth was also monitored by CONTIN analysis (data not reported). This showed that

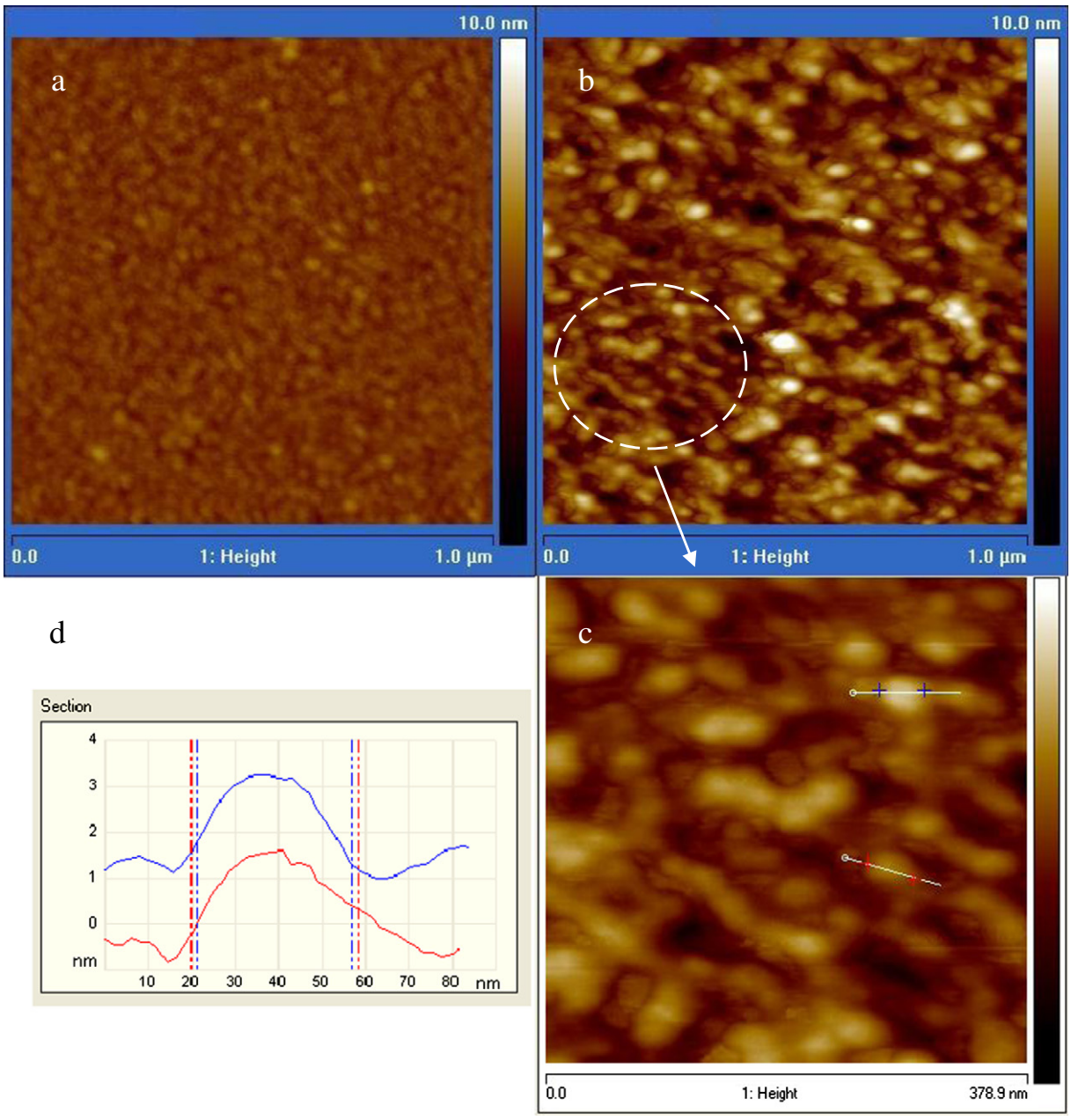

Fig. 2. AFM images (height data) of SolC samples at room temperature before (Panel *A*) and after 4 h (Panel *B*) of incubation at 56 °C; *Panel C*: Zoom of the image reported in B; *Panel D*: Cross sections of the image reported in panel C, in connection to the white lines. Red and blue vertical lines report the position of the red and blue crosses on the image in panel C.

during the early stage of the kinetics, after thermal equilibrium, all samples had one component with a diameter of about 4 nm, attributed to the lysozyme monomer [59]. Afterwards, the evolution changed according to the protein concentration. Formation of large species with a diameter of hundreds of nanometers was observed after the lag phase in all analyzed samples. In particular, dimension and number were greater in samples with a higher initial concentration.

3.1.2. Morphology characterization

In order to obtain information on the morphology of the species created in our experimental conditions, AFM measurements were performed. Fig. 2a and b show AFM images of native and aggregated (after 4 h at 56 °C) SolD sample. Comparison between the two images evidences that incubation at 56 °C led to the formation of large species made up of agglomerated units having a globular conformation with a mean diameter of about 30–40 nm (Fig. 2c–d). Moreover, fibrillar structures were not present in the field of view observed, though some elongated structures were revealed. As better shown by a zoomed image in Fig. 2c, these structures consisted of oligomers fused along their high-curvature perimeter and formed strings of aggregates. This also suggested that, in our experimental conditions and over the time monitored here, the aggregation process of lysozyme at pH 7.4 did not involve the formation of fibrils, though the hypothesis that they may be formed at a later stage cannot be excluded.

3.1.3. Thermal quenching experiments

The presence of a lag phase in the aggregation kinetics of lysozyme at physiological pH and T = 56 °C suggested the occurrence of a nucleation process driving the aggregate growth. Bearing in mind that, in nucleation processes, temperature affects the rate of the elongation

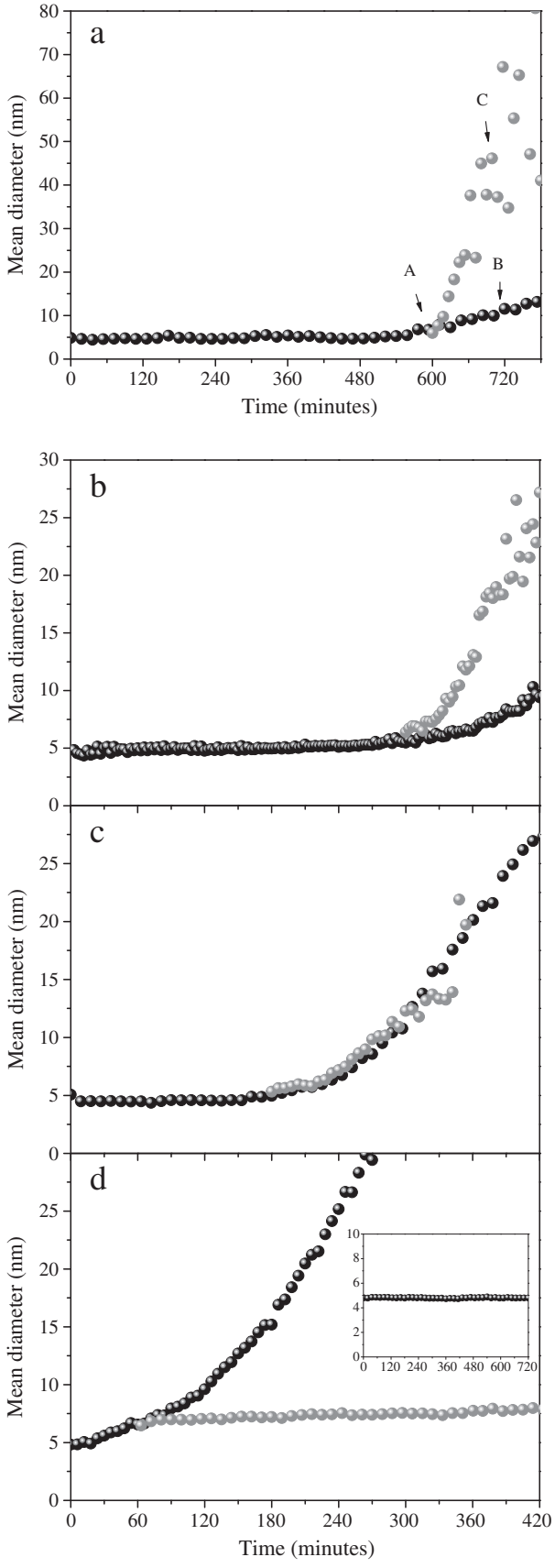

phase, in order to highlight the dependence of the aggregation on temperature, we performed specific DLS kinetics studies, referred to herein as thermal quenching experiments, to study the evolution of aggregation at room temperature (25 °C), after incubation at 56 °C. In particular, after a specific time of incubation, the temperature of the protein solution was immediately decreased to 25 °C and the evolution of the aggregate growth was followed and compared with the peculiar evolution at 56 °C. For SolA, SolB and SolC, the time point at which the solutions were cooled at 25 °C was chosen for each sample as the moment when the Z-average increased markedly, at the end of the lag-phase. First, it has to be underlined that after cooling a further evolution in mean diameter growth was expected when quenching was performed after nuclei formation, since nuclei elongation and thickening are diffusion-limited and autocatalytic processes [48,58,60]. By contrast, in the absence of nuclei formation, the aggregation process could not be activated and the signal remained unchanged.

In Fig. 3, the time evolution of the mean dimension of the particles within the protein solution incubated at 56 °C and subject to quenching at 25 °C is reported for all samples having a different protein concentration. Cooling was performed for each sample at the time point where the mean diameter increased markedly, i.e. at the end of the lag phase for SolA, SolB and SolC: this explains why the incubation time for the protein solution at 56 °C was different for each sample (SolA: 600 min, SolB: 240 min, SolC: 180 min and SolD: 60 min). It is noteworthy that the modifications in size observed when the protein was incubated at 56 °C had to be attributed to the heating. Indeed, the high stability of native lysozyme was proven at all concentrations investigated. In particular, in the inset in Fig. 3d, we show that the mean molecule diameter in the high concentration sample (SolD), incubated at 25 °C for 720 min, remained unchanged.

The time evolution of the mean diameter in the graphs highlights that for SolA (Fig. 3a) the aggregate growth kinetics was not stopped by decreasing the temperature from 56 to 25 °C. Indeed, as also verified by AFM measurements shown below (Fig. 5), the decrease in temperature favored the formation of larger aggregates, for the same monitoring times, compared with aggregates of SolA formed after complete incubation at 56 °C. Usually, a rapid increase in mean diameter after a lag phase, due to the elongation of the nucleus, is the second phase of a nucleation process [27,30,57,58]. This phase is autocatalytic [58]. Our results for SolA showed that a temperature decrease promoted the nucleation process. We can also state that other thermal quenching experiments (data not reported), carried out by cooling the SolA protein solution before 480 min of incubation at 56 °C, did not show this steep increase. This indicated that formation of small aggregated structures (acting as building blocks) with a crucial dimension was a necessary condition to induce the formation of supramolecular aggregates and revealed the occurrence of a nucleation process at the basis of the aggregate growth. Similar behavior was also observed for the SolB sample (Fig. 3b). However, in this case, the rate of the growth step occurring at 25 °C in SolB, if compared to that of SolA, decreased slightly, indicating that it decreased with an increase in native protein concentration.

Regarding SolC, the course of mean diameter is reported in Fig. 3c. Data showed that cooling at 25 °C after incubation for 180 min at 56 °C did not affect the evolution of the mean diameter of the aggregates as a function of time, indicating that aggregate growth, as revealed at 56 °C, proceeded independently of temperature. Also in this sample, the crucial conditions for the evolution of aggregation occurred before cooling, thus allowing the elongation of the nuclei via the second step

Fig. 3. Time evolution of the mean diameter of the aggregates for (*panel a*) SolA, (*panel b*) SolB, (*panel c*) SolC and (*panel d*) SolD samples, as obtained by Cumulant analysis of DLS data. Symbols: (●) whole kinetics at 56 °C; (○) kinetics at 25 °C after 600 min for SolA (*a*), after 240 min for SolB (*b*), after 180 min for SolC (*c*) and after 60 min for SolD (*d*) of incubation at 56 °C. Arrows A, B and C in *panel a* indicate the times at which the kinetics were interrupted in order to take the AFM images shown in Fig. 5. Finally, the inset in *panel d* shows the whole time evolution of the mean diameter of the protein molecules in native SolD kept at 25 °C.

of the nucleation process. In SolD, the higher concentration sample for which the existence of a lag phase cannot be stated by the evolution of the light scattered intensity and of the mean diameter reported in Fig. 1a and b, cooling stopped the evolution of the aggregation process (Fig. 3c). Since in almost all data shown above, the growth step occurring after the lag phase is an autocatalytic and diffusion-limited process, we can affirm that the mechanism driving the aggregation process of lysozyme at physiological pH is nucleation. Also, the behavior of SolD may be coherent with this claim, if we consider that the sudden growth in the scattering signal and consequently in mean diameter may be due to fast, efficient formation of nuclei. In other words, the lag phase was hidden because of the high concentration of the sample. In this case, the end of diameter growth observed in our results can be explained by considering that lowering temperature reduces particle mobility and that both nucleation and growth are hindered. However, it should be underlined that this interpretative scheme holds good when the process is diffusion-promoted, and not diffusion-limited as the nuclei elongation and thickening processes are.

In order to clarify this issue, incubation of SolD was performed at 54 and 52 °C to slow down the protein aggregation process and so to clarify whether or not there is a lag phase. The data, reported in Fig. 4, show that the initial mean diameter was the same in all cases, corresponding to the diameter of the native species. On lowering the incubation temperature from 56 °C to 54 °C, we revealed that aggregate growth was once again immediate, but at a lower rate. At 52 °C, no changes were observed, indicating that this temperature was much low to activate the SolD aggregation process at physiological pH. No lag phase was revealed for the aggregation process of lysozyme at 60 mg/ml in any of the cases examined. Our findings show that, on the one hand, a nucleation process drove the aggregation process of lysozyme more efficiently at low than at high concentration. On the other hand, results obtained on SolD highlight that the aggregation process at high concentration was not easily explainable with the nucleation model alone.

In order to explore the effects of temperature modifications on the morphology of the aggregates after nuclei formation, AFM images obtained from SolA, were acquired at room temperature: the AFM images were acquired after incubation at 56 °C for 10 h (Fig. 5a), for 12 h (Fig. 5b) and for 10 h followed by incubation at 25 °C for the next 2 h (Fig. 5c). The interruption times for the DLS kinetics of SolA are highlighted in Fig. 3a by arrows A, B and C, respectively. At these same times, DLS distributions were calculated (Fig. 6). Fig. 5a reports the image taken at the time indicated by arrow A in Fig. 3a; it shows that very few oligomeric species with a dimension of between 20 and 50 nm were formed in solution. Among them, the bigger oligomeric species of about 50 nm probably constituted the building blocks for the nucleation process. The effect of cooling the protein solution to 25 °C

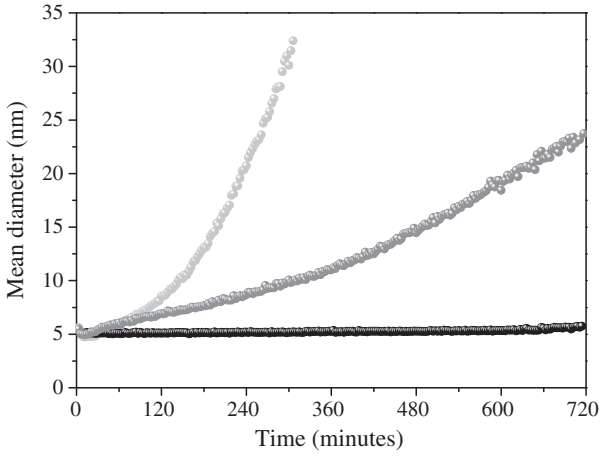

Fig. 4. Time evolution of mean diameter of the particles in SolD at 52 °C (●), 54 °C (◉) and 56 °C (○). The pH value was 7.4.

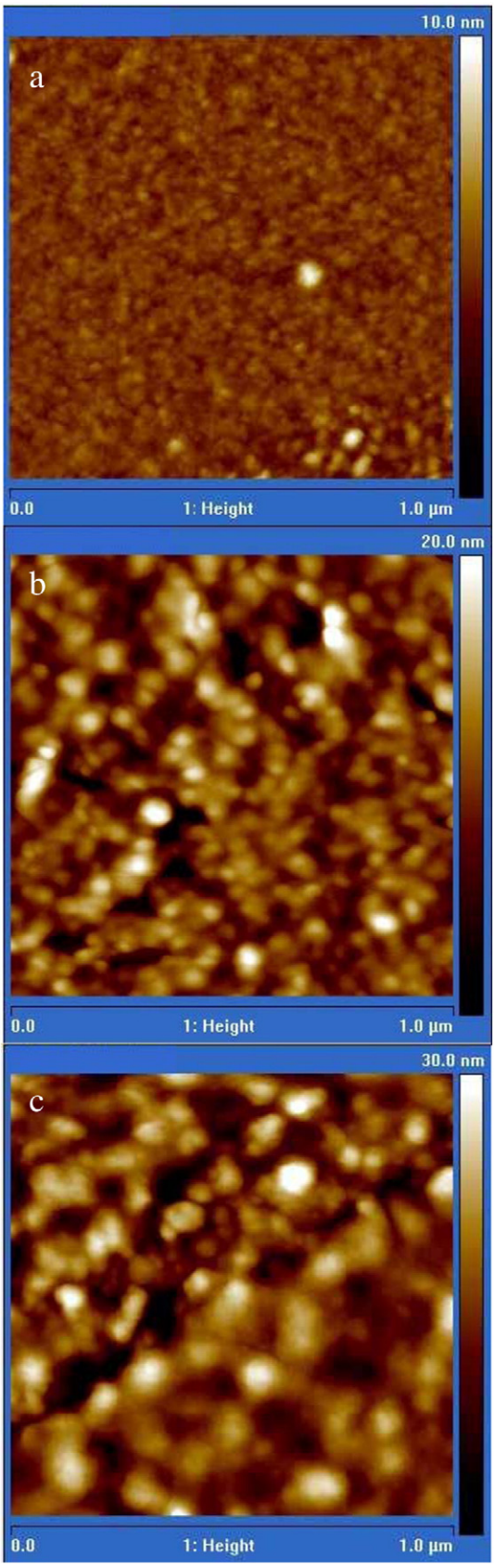

Fig. 5. AFM images (height data) of SolA sample (*panel A*) after 10 h at 56 °C, (*panel B*) after 12 h at 56 °C and (*panel C*) after 10 h at 56 °C + 2 h at 25 °C.

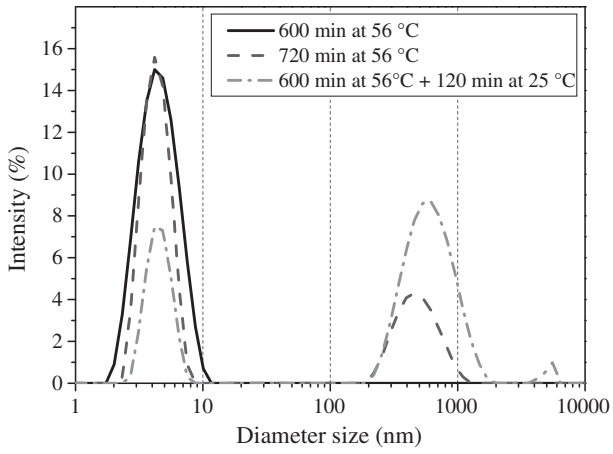

Fig. 6. Size distribution of the protein molecules in solution of SolA as obtained by DLS data after 600 min at 56 °C (black continuous line), after 720 min at 56 °C (dark gray dashed line) and after 600 min at 56 °C + 120 min at 25 °C (gray dash-point line).

(after incubation at 56 °C) is evident on comparing the images in Fig. 5b and c, acquired respectively after stopping the thermal kinetics at the time points indicated by arrows B and C in Fig. 3a. Globular aggregates formed after continuous incubation at 56 °C (Fig. 5b) were made up of subunits with an apparent mean diameter of about 40 nm, while more numerous amorphous aggregates in Fig. 5c, formed after cooling down the sample to 25 °C, were made up of units with an apparent mean diameter of about 55–60 nm. Further, some globular aggregates with a much greater three-dimensional size (order of μm) were imaged for SolA after cooling to 25 °C, but these unclear images were not reported due to a limit in the AFM technique. It is worthwhile stressing that, in all the samples investigated, no fibrils were revealed in the several zones imaged by AFM.

The size distributions calculated by CONTIN analysis of the scattering data at the same time points indicated by the arrows in Fig. 3a, consistently with the AFM findings, prove that cooling (C time in Fig. 3a and dash/point/dash line in Fig. 6) induced an increase in the number of species, with a shift in the distribution towards larger dimensions (at about 600 nm) and the appearance of a species of some micrometers in length. Indeed, incubation at 56 °C after 12 h (arrow B in Fig. 3a) caused elongation with the faint appearance of a species of about 600 nm (dashed line in Fig. 6). After 10 h at 56 °C and the next 2 h at 25 °C (dash/point/dash line in Fig. 6), a decrease in the number of native species was revealed, with more larger species being formed. Based on the AFM images and size distribution, we identified the species at about 600 nm as arising from the association of high-molecular-weight oligomers.

3.2. Conformational changes

Conformational changes of the secondary and tertiary structures accompanying the early stages of the lysozyme aggregation process were characterized using FTIR absorption spectroscopy. The Amide I vibrational band of the polypeptide chain has a composite profile consisting of several spectral components related to the different types of secondary structures [19,20,51–54]. Usually, during incubation, we follow the evolution of Amide I to detect the conformational changes of the protein secondary structure. Moreover, the Amide II (II′) band, due to N–H (or D) in-plane bending of the peptide groups [56], is related to conformational changes of the tertiary structure. In particular, the time evolutions of these band profiles give information on the protein unfolding with consequent H–D exchange between protein and solvent [16,18–20,50].

Independently of the concentration, the trend of the changes and the times characterizing the kinetics evolution were similar in all

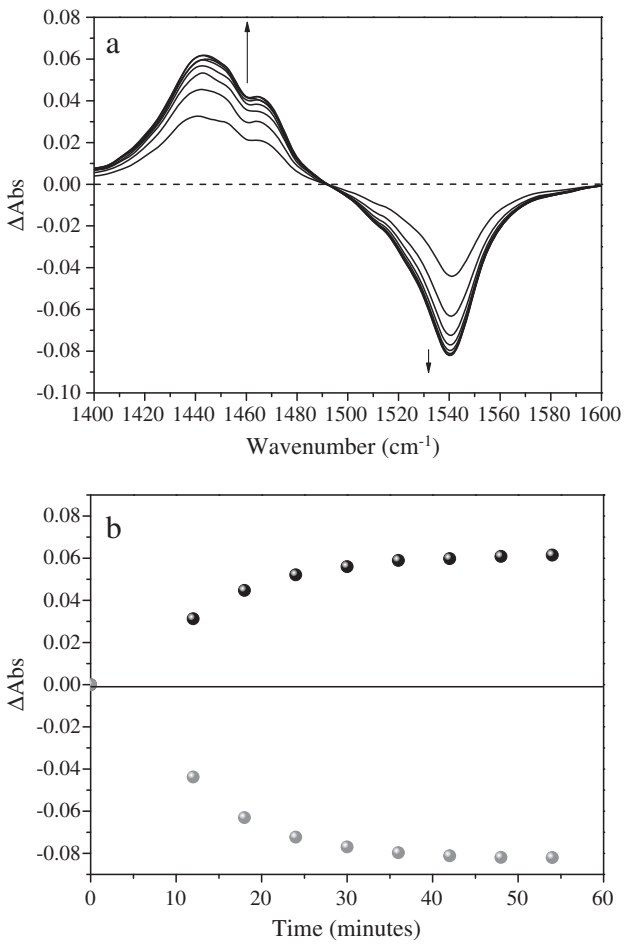

Fig. 7. (*a*) Differential absorption spectra of the SolC sample at different times of incubation at 56 °C in the Amide II and Amide II′ spectral region. (*b*) Time evolution of differential absorption intensity at 1445 cm^{-1} (●) and at 1540 cm^{-1} (○). The arrows indicate the band evolution as a function of the time.

samples. We therefore show the spectra of SolD which has the best signal/noise ratio since this sample has the highest concentration investigated. In Fig. 7a, the differential infrared absorption spectra of the SolD sample, acquired at different times, are reported in the spectral range of Amide II and Amide II′. The time evolution of the partial unfolding of the protein, as revealed by the progressive decrease of Amide II in favor of Amide II′, can be clearly deduced from Fig. 7b; it is evident that this conformational change at tertiary structure level was completed in the first 40 min of the kinetics.

By analyzing the Amide I region (Fig. 8a), three negative components and one positive component were clearly noted. The components at about 1673 and 1685 cm^{-1} were assigned to vibrations in β-turn structures, the component at about 1655 cm^{-1} was attributed to vibrations in α-helix structures, and the component at 1638 cm^{-1} was due to the vibrations in intramolecular β-sheets. Therefore, the stable high temperature induced a conversion of β-turn and mainly α-helix structures into intramolecular β-sheets [51,52]. The absence of a component at about 1620 cm^{-1} indicated that the aggregation did not proceed via formation of β-aggregated structures, unlike what occurred at a temperature above 75 °C [61,62]. This suggests that hydrophobic interactions were at the basis of the aggregate growth. The time evolution of the conformational changes, reported in Fig. 8b for SolD (analogous to that observed for SolA, SolB and SolC), showed that the changes induced by incubation at 56 °C on the protein secondary structures were completed in the first 40 min of the kinetics, simultaneously to the changes in the tertiary structures. This behavior has already been observed in other protein systems and reported in previous papers of ours [16,18,19].

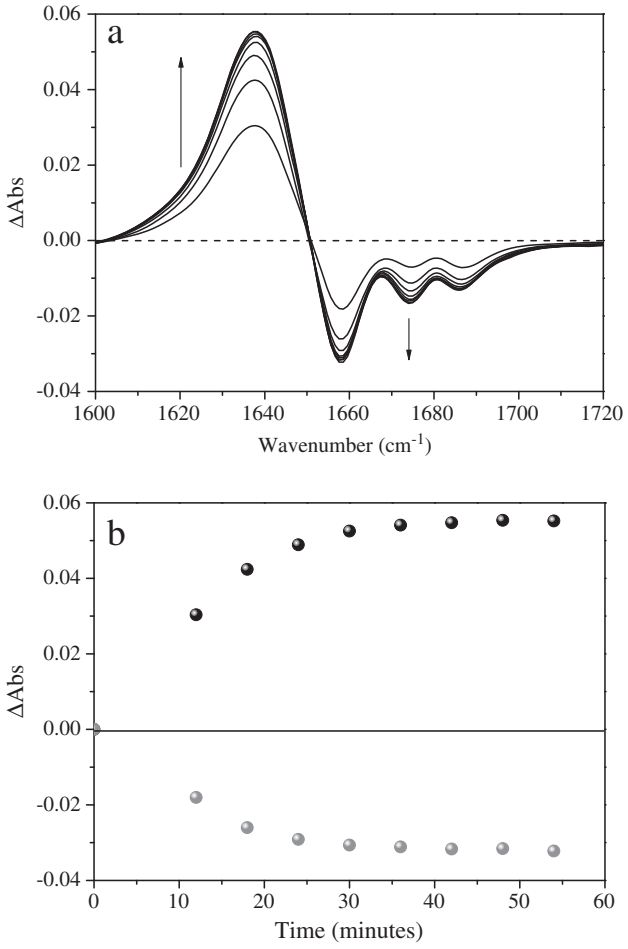

Fig. 8. (*a*) Differential absorption spectra of the SolC sample at different incubation times at 56 °C in the Amide I′ spectral region. (*b*) Time evolution of differential absorption intensity of Amide I′ components at 1638 cm^{-1} (●) and at 1657 cm^{-1} (○). The arrows indicate the evolution of the components as a function of time.

The conformational changes that the protein underwent as a consequence of incubation occurred at times that enable us to affirm that in SolA, SolB and SolC, they were well separated in time compared to the nuclei formation and subsequent elongation (see Fig. 1). We therefore suggest that the protein conformation revealed by FTIR spectroscopy is that of the nuclei constituting the building blocks of the final aggregate formation. This characterization may be relevant for studies comparing the toxicity of oligomers to their conformation, analogously to what has been reported for other studies performed under different experimental conditions [31,34,63].

4. Discussion

DLS data collected at concentrations of 10, 20 and 30 mg/ml (SolA, SolB and SolC) showed that, during the monitoring period, the aggregation process of lysozyme at pH 7.4 was a biphasic process, including different mechanisms in different spatial and time scales. The early stage was characterized by conformational rearrangements of the protein and by the formation of small oligomeric structures, occurring during the lag phase. Such structures constituted the nuclei for the formation of supramolecular aggregates during the second phase of the process. So, in our experimental conditions, as evidenced by the presence of a lag phase, whose duration depended on the initial monomer concentration, a nucleation process contributed to the formation of supramolecular aggregates. Indeed, during the lag phase, partially denatured proteins interact to form a critical nucleus constituting the building block for aggregate growth. Nucleation, homogeneous rather than heterogeneous, is an infrequent event because it implies the simultaneous interaction of intermediates and the overcoming of a free energy barrier by concentration statistical fluctuations. This mechanism, like all aggregation mechanisms, is affected by the protein concentration in solution [30]. The initial concentration essentially determines the volume each molecule has to "wander around in" with consequences on the protein–protein interactions [27]. In particular, on increasing the initial monomeric concentration, the size of the nuclei increases while the lag time decreases [58]. Coherently with this theory, in our study the lag time decreased with the increase of the monomeric concentration (Fig. 1), suggesting that a nucleation process occurred to form lysozyme aggregates. After nuclei formation, the nucleation model predicts an explosive autocatalytic appearance of aggregates [58]. The thermal quenching experiments clearly highlighted that, for some samples (SolA and SolB), the second phase of the aggregation process was autocatalytic. Indeed, the temperature decrease caused an increase in the elongation rate in SolA and SolB but no effect on the evolution of SolC, while it stopped the aggregation process in SolD. These results show that the autocatalytic process became less efficient on increasing sample concentration and disappeared in SolD. On the one hand, these data could be explained considering that particle mobility reduces and that both nucleation and growth are hindered when the temperature is lowered. This effect may be enhanced at higher protein concentrations. In actual fact, in samples prepared at higher monomer concentrations, nucleation efficiency was lower. On the other hand, the data could be understood by hypothesizing the presence of a non-nucleative and a diffusion-controlled aggregation process occurring simultaneously with the nucleation that prevails on increasing protein concentration, when the thermodynamic tendency of the molecules to aggregate increased, due to the consequent protein–protein interactions, thus hindering the growth of the nuclei. In our opinion, supported by the results obtained by incubating SolD at lower temperatures, this second hypothesis is the more reliable. Indeed, where only one mechanism drives aggregate growth, i.e. the nucleation process revealed at lower concentrations, in SolD, where a lag phase is not revealed, nuclei have to form faster and more efficiently than in other samples. Given that protein incubation at 56 °C was interrupted when average diameter had markedly increased and so when the elongation phase had already started, and hypothesizing that the nucleation process was the sole process driving the aggregation, we were unable to explain why the aggregate growth was interrupted when temperature was decreased to 25 °C. So, we believe that the behavior of SolA, SolB and SolC in thermal quenching experiments clearly highlights the occurrence of a nucleation process, whose efficiency decreased as the protein monomer concentration increased. The behavior of SolD revealed the reasons for the lower efficiency of the nucleation process. The fact that the aggregate growth was interrupted as a consequence of cooling the sample indicated that nuclei were absent or did not have the critical size necessary to start the autocatalytic elongation phase. So, in SolD, a non-nucleative process promoted by the molecular diffusion drove the aggregate growth via homogeneous association of monomers and/or oligomers. As expected, this process was enhanced when concentration and temperature were higher. In the light of these considerations, the behavior of SolC compared to SolA and SolB, where the protein cooling did not modify the evolution of lysozyme aggregation revealed at 56 °C, seems to highlight the co-existence of at least two different aggregation processes, one prevailing over the other according to the extant protein concentration. Although further investigations will have to be carried out in order to clarify the nature of the second process involved in lysozyme aggregation at physiological pH, our data demonstrate that nucleation cannot be the sole process driving the formation of mature aggregates in the protein.

Moreover, the thermal quenching experiments provided results consistent with some aspects of the nucleation model [27]. As mentioned above, incubation at 56 °C of all the samples decreased the elongation rate with the increase in the initial monomer concentration and with the decrease in the lag-time, while by contrast the thermal quenching experiments showed that after cooling the elongation rate increased

when the initial monomer concentration decreased. These results can be interpreted by relating the observed behavior with the dependence of the nuclei elongation rate on the nuclei concentration formed during the lag phase. So, we can speculate that as the monomer concentration increased, a lower concentration of nuclei was progressively formed during the lag phases. This effect may be related with the existence of the second process, whose efficiency increased on increasing the protein concentration, thus progressively hindering the formation of nuclei.

It should be underlined that the lysozyme nucleation process has already been studied at acidic pH [31,35] and at basic pH near to the protein isoelectric point [4], but has never been described at physiological pH.

AFM measurements, performed after the beginning of the elongation process (C and B in Fig. 3a), have shown the presence of oligomeric structures made up of units of about 50 nm in size (Fig. 5b and c). This proved that oligomer formation did not proceed markedly during elongation, in agreement with the model of oligomers as nucleation sites and predicting that protofibrils or aggregate formation via nucleation begins in lock step with oligomer formation [31]. Since the native lysozyme shape is associated with an ellipsoid having volume $(\pi/6) \times 4.5 \times 3.0 \times 3.0\ nm^3$ [59] and gyration radius of 1.64 nm at 20 °C and pH 7.2 [64], AFM images revealed that oligomer formation stopped after the association of about 15 monomers. We identified these oligomers as the nuclei or building blocks that in SolA and SolB set off the formation of supramolecular aggregates via nucleation. We then noted that the dimension of these peculiar oligomers formed during the lag phase in SolA and SolB was very similar (Fig. 1a), although the thermal quenching experiments proved that the efficiency of the nucleation process appeared higher in SolA. Therefore, in agreement with what was discussed above, we can now affirm that a longer lag-time (about 600 min for SolA compared to 180 min for SolB) led to the formation of more numerous nuclei, homogeneously distributed in the protein solution. This scenario implies that oligomer formation probably represents the rate-limiting step for the second step in the nucleation process. In addition, AFM images did not reveal any fibril formation.

In this respect, it may be of interest to characterize the conformation of the different aggregative states in order to highlight the underlying causes for the evolution of the aggregation process towards different pathways, amorphous aggregate or fibril formation. Concerning the conformation of lysozyme aggregates, it is noteworthy that the morphology of the oligomers characterized here is strictly analogous to that of the toxic oligomers formed by lysozyme during incubation at acidic pH [31]. The formation of these toxic oligomers constituted the creation of the nuclei leading to the formation of protofibrils and fibrils via the contribution of a nucleation process [31,65].

The details on the conformational properties driving oligomer formation lead us to speculate on the FTIR results. Analysis of the FTIR kinetics showed the changes of the secondary and tertiary structures occurring simultaneously, and concluding within the first 40–50 min of incubation at 56 °C. Considering that, at low concentrations, nuclei formation occurred from 120 min onwards, this indicates that the protein conformation characterized by FTIR spectroscopy is the same as that of the building blocks for the nucleation process occurring in Lysozyme. In particular, the monomer association for forming oligomeric nuclei was related to a partial unfolding of the native tertiary structure of the monomers and was associated with a decrease in α-helix structures in favor of intramolecular β-structures. In general, the oligomers leading to fibril formation, when incubated at high temperature show a drop in α-helix structures and the appearance of the component attributed to the formation of intermolecular β-structures typical of amyloid fibrils [6,8,25,34]. Moreover, when the lysozyme aggregation process occurs in acidic conditions, the amount of β-structure in the aggregates increases even though the entire polypeptide chain is not involved in this type of structure [63]. The lack of intermolecular β-structures, proving the absence of β-like aggregates, is the main difference encountered in the comparison between the conformation and morphology of the oligomers studied here at physiological pH and those leading to the formation of protofibrils and mature fibrils at acid pH [63]. This lack is no doubt related with the formation of amorphous aggregates instead of fibrils, as also observed by our AFM images. Notwithstanding, it should be borne in mind that, even though no fibrillar structures were revealed in any of the samples investigated, some elongated structures were formed by oligomer association. The possibility that these structures could be protofibrils, characterized by the formation of intermolecular β-structures typical of amyloid fibrils, was not supported by our data. However, it should be remembered that species with very low concentrations might not be revealed by FTIR spectroscopy. So, a possible coexistence between amorphous and a few proto-fibrillar aggregates under the experimental conditions implemented here cannot be excluded. In every case, however, our data showed that the aggregative state moves towards a globular mature aggregate rather than towards a fibrillar one.

The analogy between the morphology of the oligomers analyzed in this study and those constituting toxic protofibrils in fibrillar association of lysozyme at acidic pH, suggests the need to carry out toxicity experiments in our experimental conditions.

5. Conclusions

In this paper, we studied the thermal aggregation process of lysozyme at physiological pH by DLS and FTIR absorption kinetics and AFM. By changing the concentration and the temperature of the protein, we characterized the nucleation process driving the formation of aggregates in Lysozyme solutions at pH 7.4. However, peer analysis of the experimental data highlighted that this process cannot be the only process involved. In particular, our results demonstrate that the occurrence of at least two different aggregation processes, a nucleation and a homogeneous diffusion-controlled process. One process could prevail over the other as a function of protein concentration. When nucleation occurred, nuclei concentration was higher in samples having a lower initial monomeric concentration and showing a longer lag-phase.

We also highlighted the structural and morphological properties of these nuclei, which, dependently on the concentration, could constitute the building blocks for the formation of amorphous aggregates. The critical size of the nuclei, identified as globular oligomeric structures, i.e. 15-mers, was at about 50 nm. From a structural point of view, study of the early conformational changes, separated in time from the formation of nuclei and mature aggregates, enabled us to characterize different conformational levels of the oligomeric state. Supramolecular aggregation proceeded without the formation of β-aggregated structures towards the growth of oligomers and amorphous aggregates; no fibrillar structures were observed.

Acknowledgments

We are grateful to all members of the MBSM group (http://www.fisica.unipa.it/biophysmol/) and in particular to Vito Foderà and Armida Torreggiani for the continuous stimulating discussions. The authors would like to thank Anthony Green for kindly reviewing the English in the manuscript.

References

[1] W. Gosal, S.B. Ross-Murphy, Globular protein gelation, Current Opinion in Colloid and Interface Science 5 (2000) 188–194.
[2] A. Clark, G. Kavanagh, S. Ross-Murphy, Globular protein gelation-theory and experiment, Food Hydrocolloids 15 (2001) 383–400.
[3] H.A. Lashuel, S.R. La Brenz, L. Woo, L.C. Serpell, J.W. Kelly, Protofilaments, filaments, ribbons, and fibrils from peptidomimetic self-assembly: implications for amyloid fibril formation and materials science, Journal of the American Chemical Society 122 (2000) 5262–5277.
[4] H. Yan, A. Saiani, J.E. Gough, A.F. Miller, Thermoreversible protein hydrogel as cell scaffold, Biomacromolecules 7 (2006) 2776–2782.
[5] H. Yan, A. Nykanen, J. Ruokolainen, D. Farrar, J.E. Gough, A. Saiani, A.F. Miller, Thermo-reversible protein fibrillar hydrogels as cell scaffolds, Faraday Discussions 139 (2008) 71–84.

[6] F. Chiti, P. Webster, N. Taddei, A. Clark, M. Stefani, G. Ramponi, C.M. Dobson, Designing conditions for in vitro formation of amyloid protofilaments and fibrils, Proceedings of the National Academy of Sciences of the United States of America 96 (1999) 3590–3594.
[7] C.M. Dobson, Protein misfolding, evolution and disease, Trends in Biochemical Sciences 24 (1999) 329–332.
[8] C.M. Dobson, Principles of protein folding, misfolding and aggregation, Seminars in Cell & Developmental Biology 15 (2004) 3–16.
[9] M. Vendruscolo, J. Zurdo, E. MacPhee Cait, C.M. Dobson, Protein folding and misfolding: a paradigm of self-assembly and regulation in complex biological systems, Philosophical Transactions of the Royal Society of London A 361 (2003) 1205–1222.
[10] M. Stefani, C.M. Dobson, Protein aggregation and aggregate toxicity: new insight into protein folding, misfolding diseases and biological evolution, Journal of Molecular Medicine 81 (2003) 678–699.
[11] V. Vetri, R. Carrotta, P. Picone, M. Di Carlo, V. Militello, Concanavalin A aggregation and toxicity on cell cultures, Biochimica et Biophysica Acta 1804 (2010) 173–183.
[12] A. Jan, D.M. Hartley, H.A. Lashuel, Preparation and characterization of toxic Aβ intermediates for structural and functional studies in Alzheimer's disease research, Nature Protocols 5 (2010) 1186–1209.
[13] J.D. Harper, S.S. Wong, C.M. Lieber, P.T. Lansbury, Observation of metastable Aβ amyloid protofibrils by atomic force microscopy, Chemistry & Biology 4 (1997) 119–125.
[14] A.J. Modler, K. Gast, G. Lutsch, G. Damaschun, Assembly of amyloid protofibrils via critical oligomers: a novel pathway of amyloid formation, Journal of Molecular Biology 325 (2003) 135–148.
[15] V. Vetri, C. Canale, A. Relini, F. Librizzi, V. Militello, A. Gliozzi, M. Leone, Amyloid fibrils formation and amorphous aggregation in Concanavalin A, Biophysical Chemistry 125 (2007) 184–190.
[16] G. Navarra, D. Giacomazza, M. Leone, F. Librizzi, V. Militello, P.L. San Biagio, Thermal aggregation and ion-induced cold-gelation of bovine serum albumin, European Biophysics Journal 38 (2009) 437–446.
[17] V. Foderà, S. Cataldo, F. Librizzi, B. Pignataro, P. Spiccia, M. Leone, Self-organization pathways and spatial heterogeneity in insulin amyloid fibril formation, The Journal of Physical Chemistry 113 (2009) 10830–10837.
[18] G. Navarra, M. Leone, V. Militello, Thermal aggregation of beta-lactoglobulin in presence of metal ions, Biophysical Chemistry 131 (2007) 52–61.
[19] G. Navarra, A. Tinti, M. Leone, V. Militello, A. Torreggiani, Influence of metal ions on thermal aggregation of bovine serum albumin: aggregation kinetics and structural changes, Journal of Inorganic Biochemistry 103 (2009) 1729–1738.
[20] P. Rondeau, G. Navarra, F. Cacciabaudo, M. Leone, E. Bourdon, V. Militello, Thermal aggregation of glycated bovine serum albumin, Biochimica et Biophysica Acta 1804 (2010) 789–798.
[21] J.P. Cleary, D.M. Walsh, J.J. Hofmeister, G.M. Shankar, M.A. Kuskowski, D.J. Selkoe, K.H. Ashe, Natural oligomers of the amyloid-β protein specifically disrupt cognitive function, Nature Neuroscience 8 (2005) 79–84.
[22] K. Garai, P. Sengupta, B. Sahoo, S. Maiti, Selective destabilization of solubile β oligomers by divalent metal ions, Biochemical and Biophysical Research Communications 354 (2006) 210–215.
[23] M.N. Vieira, L. Forny-Germano, L.M. Saraiva, A. Sebollela, A.M. Martinez, J.C. Houzel, F.G. De Felice, S.T. Ferreira, Soluble oligomers from a non-disease related protein mimic Abeta-induced tau hyperphosphorylation and neurodegeneration, Journal of Neurochemistry 103 (2007) 736–748.
[24] F. Chiti, C.M. Dobson, Protein misfolding, functional amyloid, and human disease, Annual Review of Biochemistry 75 (2006) 333–366.
[25] E. Frare, P.P. de Laureto, J. Zurdo, C.M. Dobson, A. Fontana, A highly amyloidogenic region of hen lysozyme, Journal of Molecular Biology 340 (2004) 1153–1165.
[26] J. Juarez, P. Taboada, V. Mosquera, Existence of different structural intermediates on the fibrillation pathway of human serum albumin, Biophysical Journal 96 (2009) 2353–2370.
[27] F. Ferrone, Analysis of protein aggregation kinetics, Methods in Enzymology 309 (1999) 256–274.
[28] P.T.J. Lansbury, Evolution of amyloid: what normal protein folding may tell us about fibrillogenesis and disease, Proceedings of the National Academy of Sciences 96 (1999) 3342–3344.
[29] C.J. Roberts, Kinetics of irreversible protein aggregation; analysis of extended Lumry–Eyring models and implications for predicting protein shelf life, The Journal of Physical Chemistry. B 17 (2003) 1194–1207.
[30] P. Hortschansky, V. Scroeckh, T. Christopeit, G. Zandomeneghi, M. Frandrich, The aggregation kinetics of Alzheimer's β-amyloid peptide is controlled by stochastic nucleation, Protein Science 14 (2005) 1753–1759.
[31] S.E. Hill, J. Robinson, G. Matthews, M. Muschol, Amyloid protofibrils of lysozyme nucleate and grow via oligomer fusion, Biophysical Journal 96 (2009) 3781–3790.
[32] C.C. Blake, D.F. Koenig, G.A. Mair, A.C.T. North, D.C. Phillips, V.R. Sarma, Structure of hen-egg white lysozyme, Nature 206 (1965) 757–761.
[33] M. Krebs, D. Wilkins, E. Chung, M. Pitkeathly, A. Chamberlain, J. Zurdo, C. Robinson, C.M. Dobson, Formation and seeding of amyloid fibrils from wild-type hen lysozyme and a peptide fragment from the beta-domain, Journal of Molecular Biology 300 (2000) 541–549.
[34] E. Frare, M.F. Mossuto, P.P. de Laureto, M. Dumoulin, C.M. Dobson, A. Fontana, Identification of the core structure of lysozyme amyloid fibrils by proteolysis, Journal of Molecular Biology 361 (2006) 551–561.
[35] L.N. Arnaudov, R. de Vries, Thermally induced fibrillar aggregation of hen egg white lysozyme, Biophysical Journal 88 (2005) 515–526.
[36] R. Mishra, K. Sörgjerd, S. Nyström, A. Nordigården, Y.C. Yu, P. Hammarström, Lysozyme amyloidogenesis is accelerated by specific nicking and fragmentation but decelerated by intact protein binding and conversion, Journal of Molecular Biology 366 (2007) 1029–1044.
[37] C.M. Dobson, P.A. Evans, S.E. Radford, Understanding how proteins fold: the lysozyme story so far, Trends in Biochemical Sciences 19 (1994) 31–37.
[38] D.R. Booth, M. Sunde, V. Bellotti, C.V. Robinson, W.L. Hutchinson, P.E. Fraser, P.N. Hawkins, C.M. Dobson, S.E. Radford, C.C. Blake, M.B. Pepys, Instability, unfolding and aggregation of human lysozyme variants underlying amyloid fibrillogenesis, Nature 385 (1997) 787–793.
[39] M. Muschol, F. Rosenberger, Liquid–liquid phase separation in supersaturated lysozyme solution and associated precipitate formation/crystallization, The Journal of Chemical Physics 107 (1997) 1953–1962.
[40] M. Manno, C. Xiao, D. Bulone, V. Martorana, P.L. San Biagio, Thermodynamic instability in supersaturated lysozyme solutions: effect of salt and role of concentration fluctuations, Physical Review E 68 (2003) 011904.
[41] P.R. ten Wolde, D. Frenkel, Enhancement of protein crystal nucleation by critical density fluctuations, Science 277 (1997) 1975–1978.
[42] W.C.K. Poon, S.U. Egelhaaf, P.A. Beales, A. Salonen, L. Sawyer, Protein crystallization: scaling of charge and salt concentration in lysozyme solutions, Journal of Physics. Condensed Matter 12 (2000) L569–L574.
[43] S. Goda, K. Takano, Y. Yamagata, R. Nagata, H. Akutsu, S. Maki, K. Namba, K. Yutani, Amyloid protofilament formation of hen egg lysozyme in highly concentrated ethanol solution, Protein Science 9 (2000) 369–375.
[44] Y. Yonezawa, S. Tanaka, T. Kubota, K. Wakabayashi, K. Yutani, S. Fujiwara, An insight into the pathway of the amyloid fibril formation of hen egg white lysozyme obtained from a small-angle X-ray and neutron scattering study, Journal of Molecular Biology 323 (2002) 237–251.
[45] S. Tanaka, Y. Oda, M. Ataka, K. Onuma, S. Fujiwara, Y. Yonezawa, Denaturation and aggregation of hen egg lysozyme in aqueous ethanol solution studied by dynamic light scattering, Biopolymers 59 (2001) 370–379.
[46] A. Cao, D. Hu, L. Lai, Formation of amyloid fibrils from fully reduced hen egg white lysozyme, Protein Science 13 (2004) 319–324.
[47] S. Raccosta, M. Manno, D. Bulone, D. Giacomazza, V. Militello, V. Martorana, P.L. San Biagio, Irreversible gelation of thermally unfolded proteins: structural and mechanical properties of lysozyme aggregates, European Biophysics Journal 39 (2010) 1007–1017.
[48] S. Tomita, H. Yoshikawa, K. Shiraki, Arginine controls heat-induced cluster–cluster aggregation of lysozyme at around the isoelectric point, Biopolymers 95 (2011) 695–701.
[49] W. Brown, Dynamic Light Scattering: The Method and Some Applications, Oxford University Press, New York, 1993.
[50] V. Militello, C. Casarino, A. Emanuele, A. Giostra, F. Pullara, M. Leone, Aggregation kinetics of bovine serum albumin studied by FTIR spectroscopy and light scattering, Biophysical Chemistry 107 (2004) 175–187.
[51] D.M. Byler, H. Susi, Examination of the secondary structure of proteins by deconvolved FTIR spectra, Biopolymers 25 (1986) 469–487.
[52] A. Dong, P. Huang, W.S. Caughey, Protein secondary structures in water from second-derivative Amide I Infrared spectra, Biochemistry 29 (1990) 3303–3308.
[53] S. Cai, B.R. Singh, Identification of β-turn and random coil amide III infrared bands for secondary structure estimation of proteins, Biopolymers 80 (1999) 7–20.
[54] J.T. Pelton, L.R. Mec Lean, Spectroscopic methods for analysis of protein secondary structure, Analytical Biochemistry 277 (2000) 167–176.
[55] T. Lefevre, M. Subirade, Formation of intermolecular beta-sheet structures: a phenomenon relevant to protein film structure at oil–water interfaces of emulsions, Journal of Colloid and Interface Science 263 (2003) 59–67.
[56] J.M. Bakker, C. Plutzer, I. Hunig, T. Haber, I. Compagnon, G. von Helden, G. Meijer, K. Kleinermanns, Folding structures of isolated peptides as revealed by gas-phase mid-infrared spectroscopy, ChemPhysChem 6 (2005) 120–128.
[57] F.A. Ferrone, J. Hofrichter, H.R. Sunshine, W.A. Eaton, Kinetic studies on photolysis-induced gelation of sickle cell haemoglobin suggest a new mwchanism, Biophysical Journal 32 (1980) 361–380.
[58] F.A. Ferrone, J. Hofrichter, W.A. Eaton, Kinetics of sickle hemoglobin polymerization. II. A double nucleation mechanism, Journal of Molecular Biology 183 (1985) 611–631.
[59] I.E. Dickerson, I. Geis, The Structure and Action of Proteins, Harper and Row, New York, 1969.
[60] T.A. Witten, L.M. Sander, Diffusion-limited aggregation, a kinetic critical phenomenon, Physical Review Letters 47 (1981) 1400–1403.
[61] R.I. Green, I. Hopkinson, R.A.L. Jones, Unfolding and intermolecular association in globular proteins adsorbed at interfaces, Langmuir 15 (1999) 51025110.
[62] J.Y. Chang, L. Li, The unfolding mechanism and the disulfide structures of denatured lysozyme, FEBS Letters 511 (2002) 73–78.
[63] E. Frare, M.F. Mossuto, P.P. de Laureto, S. Tolin, L. Menzer, M. Dumoulin, C.M. Dobson, A. Fontana, Characterization of oligomeric species on the aggregation pathway of human lysozyme, Journal of Molecular Biology 387 (2009) 17–27.
[64] S. Arai, M. Hirai, Reversibility and hierarchy of thermal transition of hen egg-white lysozyme studied by small-angle X-ray scattering, Biophysical Journal 76 (1999) 2192–2197.
[65] M. Malisauskas, J. Ostman, A. Darinskas, V. Zamotin, E. Liutkevicius, E. Lundgren, L.A. Morozova-Roche, Does the cytotoxic effect of transient amyloid oligomers from common equine lysozyme in vitro imply innate amyloid toxicity? Journal of Biological Chemistry 280 (2005) 6269–6275.